

J.C. Hubbert<sup>1\*</sup>, M. Dixon<sup>1</sup>, U. Romatschke<sup>1</sup>, S. M. Ellis<sup>1</sup>, C. Cappellin<sup>2</sup>, Rolf Jørgensen<sup>2</sup>

<sup>1</sup>National Center for Atmospheric Research, Boulder, CO

<sup>2</sup>TICRA Corp. Copenhagen, Denmark

## 1. INTRODUCTION

Differential reflectivity  $Z_{DR}$  calibration continues to be a challenge for weather radars and it has been difficult to achieve accuracies of 0.1 dB for NEXRAD (Ice et al. 2014). It was recently shown that  $Z_{DR}$  bias is a function of the temperature of S-Pol's (S-band Polarimetric Radar) antenna (Hubbert 2017). S-Pol is operated by the National Center for Atmospheric Research (NCAR) for the National Science Foundation (NSF). The  $Z_{DR}$  bias calculation is based on the crosspolar power technique that states

$$Z_{dr}^c = Z_{dr}^m S_1 S_2 CPR \quad (1)$$

where  $Z_{dr}^c$  is calibrated  $Z_{dr}$ ,  $Z_{dr}^m$  is experimentally measured uncalibrated  $Z_{dr}$ ,  $S_1 S_2$  is a experimentally measured V to H ratio of solar powers (see Hubbert (2017)) and  $CPR$  is the ratio of the two crosspolar powers.  $Z_{DR} = 10 \log_{10}(Z_{dr})$ . It was shown in Hubbert (2017) that the primary factor in S-Pol's  $Z_{dr}$  bias variability is S-Pol's antenna. In this paper we investigate nature of the  $Z_{DR}$  bias caused by the antenna via numerical modeling S-Pol's antenna.

A center-fed parabolic antenna reflects the wave broadcasted by the feed horn as depicted in Fig. 1. The resulting plane wave in the far field of the antenna can be thought of as the summation of individual point sources across the face of the antenna dish. The character of both the H and V antenna patterns depends directly on the relationship of the phases of these conceptual point sources. This is precisely why the phase center of the feed horn should be located at the focus of the parabola. The hypothesis is then that the relationship of the phases of the point sources is changed as the metal structure of the antenna expands and contracts with temperature.

Measurements with S-Pol have shown that the character of the antenna patterns, and consequently the  $Z_{DR}$  bias, is a function of operating frequency. Figures 2, 3 show  $S_1 S_2$  (Eq. 5) antenna patterns as

a function of the operation frequency of S-Pol over the small range of 2798 to 2805 MHz, as labeled. Fig. 4 are integrated  $S_1 S_2$  values at each frequency. The dashed red lines represent the average of the 2 or more solar scans taken at each frequency. Integrated  $S_1 S_2$  varies nearly 0.3 dB over this small frequency range! These data shows that both integrated  $S_1 S_2$  and the shape of the  $S_1 S_2$  antenna pattern are sensitive functions of small changes in operating frequency. To investigate how the antenna can affect  $Z_{DR}$  bias, we model the S-Pol antenna numerically, calculate the theoretical antenna patterns and compare them to the experimental  $Z_{DR}$  (or equivalently,  $S_1 S_2$ ) antenna patterns.

As a first order assessment of the feasibility that expansion of the metal in the S-Pol antenna could cause the seen variance in the antenna patterns, consider the phase change at the dish apex for a 1 MHz change in operating frequency: from 2800 to 2801 MHz. Taking the corresponding wavelengths and dividing them into the focal length of the parabola 381 cm (the distance from the focus of the parabola to the apex of parabola) and differencing the results yield the wavelength difference at the apex: 0.0127 wavelengths. This corresponds to a distance of 1.36 mm or a  $4.57^\circ$  phase difference. The premise is that a change in frequency, that causes an experimentally observed change in  $S_1 S_2$ , is a pseudo for the  $S_1 S_2$  variations seen with temperature change. The S-pol antenna is constructed with aluminum 6061 alloy with a expansion coefficient of  $23.6 \mu\text{cm}/\text{cm}/^\circ\text{C}$ . The support struts are about 18 feet or 548.6 cm long. Thus for a  $10^\circ\text{C}$  temperature change:  $23.6 \mu\text{cm}/\text{cm}/^\circ\text{C} \times 548.6 \text{ cm} \times 10^\circ = 1.29 \text{ mm}$ . This is of the same order as the distance 1.36 mm above. The exact nature of the antenna expansion of the S-Pol dish is quite complicated with its 28-foot dish and supporting metal cross members. For the PECAN experiment, a  $10^\circ\text{C}$  change in temperature corresponded to a change of 0.077 dB in  $Z_{dr}$  bias. While this analysis is not conclusive it does show that expansion of the S-Pol dish with temperature is a reasonable deduction.

\*NCAR/EOL, Boulder, Colorado 80307, email: hubbert@ucar.edu

## 2. NUMERICAL MODELING OF S-POL'S ANTENNA

The antenna model is analyzed in GRASP (General Reflector Antenna Software Package, by TICRA) with the Method of Moments. This is an exact full wave method, which takes into account all mutual coupling, blockage and near-field effects. The TICRA modeling includes the actual shape of the 1) dish, struts, waveguides, and feed horn. The dish shape was measured by GEODETIC cooperation of Melbourne FL in 2009 using a photogrammetry technique. Figure 5 shows the S-Pol antenna at night during the measurement process. The bright spots are about 1400 optical reflectors responding to the flash of the camera and are the measurement points. The surface RMS error across the dish was calculated to be 0.03 in. A CAD drawing of the feed horn was provided to TICRA as well as the dimensions of the struts and waveguides. Figure 6 shows the topology of the model used by TICRA including the waveguide, support struts and feed horn. The feed horn, as described by the CAD file, was placed so that the distance from the horn's *phase center* to the reflector apex was 149.51 in. This is the measured length to S-Pol's feed horn phase center. The antenna pattern of the feed horn as determined with GRASP was cross-checked with the pattern of the feed horn in CHAMP (Corrugated Horn Analysis by Modal Processing; also by TICRA), an alternative software for feed modeling with circular symmetry, and the results coincided.

Four case are modeled:

1. Full Model
2. Without waveguide
3. Without absorber
4. Horn moved 3 mm closer to the antenna reflector

The location of the phase center of the feed horn is a function of frequency as show in Fig. 7. The phase center of the feed horn ideally should be placed at the focus of the parabolic reflector antenna.

### 2.1. Model Results

One objective is to compare S-Pol's solar scans of  $S_1S_1$  to the GRASP modeled results of the  $Z_{DR}$  bias antenna pattern (defined below). To do this, the GRASP modeled antenna patterns need to be convolved with the solar disk. Shown in Fig. 8 is an H modeled antenna pattern on the left and the corresponding H antenna pattern after convolution

with the solar disk on the right. On the left image is shown a  $0.53^\circ$  solar disk (Tapping 2001). The solar disk is passed over the image and data falling into the disk are averaged. The result is a smoothed antenna pattern.

The modeled antenna patterns are analyzed for  $Z_{DR}$  bias ( $Z_{DR}^b$ ) and ICPR (Integrated Cross-Polarization Ratio) both of which are given in Chandrasekar and Keeler (1993) as

$$Z_{dr}^b = \frac{\int |f_{HH}^2 + f_{HV}^2| d\Omega}{\int |f_{VH}^2 + f_{VV}^2| d\Omega} \quad (2)$$

$$ICPR = \frac{\int |f_{HH}f_{VH} + f_{HV}f_{VV}|^2 d\Omega}{\int |f_{HH}^2 + f_{HV}^2| d\Omega} \quad (3)$$

where  $f$  are the antenna patterns expressed in

$$\begin{bmatrix} E_H \\ E_V \end{bmatrix}_t = C \begin{bmatrix} f_{HH} & f_{HV} \\ f_{VH} & f_{VV} \end{bmatrix} \begin{bmatrix} E_H \\ E_V \end{bmatrix}_a \quad (4)$$

where  $E_a$  is the field applied to the antenna and  $E_t$  is the transmitted field (Chandrasekar and Keeler 1993).  $C$  is a constant and is not important to this analysis. The ICPR is a measure of the antenna limit for LDR (Linear Depolarization Ratio), i.e., it is a measure of what the experimental LDR would be for spherical scatterers (e.g., in very light rain with only spherical particles).

Figures 9 and 10 show the  $Z_{DR}^b$  antenna patterns for the TICRA "Full Model" case convolved with the solar disk at the 10 frequencies 2801 to 2810 MHz. Compare these two figures to the experimental data of Figs. 2 and 3. In the experimental data  $S_1S_2$  becomes fairly flat at the center of the pattern for frequencies 2800 and 2801 MHz whereas for the modeled data it is flattest for frequencies 2803 and 2804 MHz. Before and after those frequencies, both  $S_1S_2$  and  $Z_{DR}^b$  become must less "flat" within the  $2^\circ$  solid angle and possess a more hour glass shape. It is remarkable that the model has captured the shapes of the experimental data and that the shape of the  $Z_{DR}$  antenna pattern changes for 1 MHz changes in frequency.

To gain further insight on  $Z_{DR}^b$  for the 4 Cases, integrated  $Z_{DR}^b$  is shown in Fig. 11 as a function of frequency. Since we are interested in antenna performance in precipitation, the following calculations are performed on the modeled data without the solar disk convolution. As can be seen,  $Z_{DR}^b$  changes very little over the plotted frequency range. This then does not explain the relatively large  $Z_{DR}^b$  changes seen in the experimental data of Fig. 4

where  $S_1 S_2$  (equivalent to  $Z_{DR}^b$ ) varies by 0.3 dB!  $S_1 S_2$  is define as (Hubbert 2017)

$$S_1 S_2 = \frac{(G_V^A W_V LNA_V C_V^R)^2 \Gamma_{co,V} \Gamma_{x,V}}{(G_H^A W_H LNA_H C_H^R)^2 \Gamma_{co,H} \Gamma_{x,H}}, \quad (5)$$

where  $C_{H,V}^R$  are the losses associated with the circulators on reception,  $W_{H,V}$  are waveguide losses,  $G_{H,V}^A$  are the antenna gains,  $LNA_{H,V}$  (low noise amplifier) are the  $LNA$  gains, and  $\Gamma$  represents the insertion losses associated with various paths through the intermediate frequency (IF) switch. The effects of  $\Gamma$  are negligible and can be ignored. Note that  $S_1 S_2$  is not only a function of the antenna gains but also the  $LNA$  gains and circulator losses,  $C_{H,V}^R$ . Thus, the differential gain of the  $LNAs$  and circulators were experimentally measured as a function of frequency and are shown in Fig. 11 with accompanying block diagram in Fig. 12. The top panel of Fig. 11 is the H to V differential gain of the S-Pol circulators through the TR limiters (i.e., from port 1 to port 2 in Fig. 12), while the bottom panel shows the H to V differential gain of the S-Pol circulators through the  $LNAs$ . The differential gain path of top panel is included in the bottom panel plot. Though not conclusive at this point, there does appear to be significant variation in the differential gain of these components as a function of frequency and this then would explain the experimental variation in  $S_1 S_2$  of Fig. 4.

## 2.2. Integrated Cross-Polarization Ratio

Integrated Cross-Polarization Ratio (ICPR) is an important figure of merit for an antenna and it is a measure of the cross-coupling between the H and V channels of the antenna, i.e., the antenna errors. In Wang and Chandrasekar (2006) and supported in Hubbert et al. (2010b,a), if the  $Z_{DR}$  bias is to be held to within 0.2 dB for the worst case scenario, then the ICPR should less than -44 dB. However, it was argued in Wang and Chandrasekar (2006) that -40 dB would be sufficient for most radar operations. ICPR “antenna patterns” are given in Figs. 13 and 14 for the Full Model case for frequencies 2801 to 2810 MHz. The ICPR patterns are calculated from the numerator of Eq.(3) for each point and normalized by denominator integral. The ICPR patterns show the relative contributions to integrated ICPR (i.e., Eq.(3)). The regions in red color scale are where maximum cross coupling occurs.

Figure 15 shows ICPR for the 4 cases as a function of frequency. ICPR is a strong function of frequency, changing by 9 dB and more over the small frequency range of 2800 to 2810 MHz. The fig-

ure shows the complex behavior of ICPR for the 4 cases. One can see that moving the phase center just 3 mm closer to the dish is the most significant effect of the 4 cases. For Fig. 15, good operating frequencies for ICPR are 2801 to 2803 MHz.

These figures indicate that ICPR for the WSR-88DPs is likely to be highly variable since the WSR-88DP frequencies vary widely across the S-band frequency range.

## 3. DISCUSSION AND CONCLUSIONS

This is the first time we know of that the copolar as well as crosspolar *complex* antenna patterns of a weather radar have been modeled in such a precise fashion. Having the complex antenna patterns allows for the  $Z_{DR}^b$  bias and ICPR to be calculated with the equations in Chandrasekar and Keeler (1993), repeated here as Eqs.(2) and (3). Previously, typically only the power patterns were available so that approximations needed to be made when using Eqs.(2) and (3).

Experimental data with S-Pol, e.g., Figs. 2, 3 and 4, have shown a dependence not only on temperature but also on frequency of operation. It is noteworthy that the  $Z_{DR}$  *antenna pattern shape* and the *system differential gain*, manifest by  $S_1 S_2$ , varies considerably for not only antenna temperature change but also small changes in operation frequency.

The modeling was able to reproduce the antenna pattern shape changes observed in the experimental data. Small changes in operating frequency, 1 MHz or 0.04%, caused the shape  $Z_{DR}$  antenna pattern to change; however, the antenna differential gain did not change appreciably over the frequency range 2801 to 2810 MHz. Experimental measurements showed that the high frequency components of S-Pol’s receiver chain (i.e.,  $LNAs$ , circulators  $C^R$ , filters, and possible the mixers) are responsible for the experimentally observed differential gain variability. However, the differential gain of S-Pol’s antenna as a function of antenna temperature is still an actuality as shown by Hubbert (2017). One can conclude that expansion/contraction of the entire antenna causes both an antenna pattern change as well as a differential gain change. Components such as the  $LNAs$  and circulators have temperature dependent gains but they are housed in a temperature controlled environment. In Hubbert (2017) it is shown that these components are not responsible for S-Pol’s  $Z_{DR}$  bias variability during PECAN and MASCRAD.

Moving the phase center of the feed horn just 3 mm closer to the dish also causes discernible differences in the antenna patterns and especially ICPR. ICPR is also a strong function of frequency varying about 10 dB or more over the 10 MHz range modeled. Thus, selecting the appropriate frequency or placing the phase center of the feed horn judiciously can have significant implications on the amount of antenna inter-channel isolation and thus on observed  $Z_{DR}$  bias variation (Wang and Chandrasekar 2006; Hubbert et al. 2010b,a).

**Acknowledgment** This research was supported in part by the ROC (Radar Operations Center) of Norman OK. The National Center for Atmospheric Research is sponsored by the National Science Foundation. Any opinions, findings and conclusions or recommendations expressed in this publication are those of the authors and do not necessarily reflect the views of the National Science Foundation.

## References

- Chandrasekar, V. and R. Keeler, 1993: Antenna pattern analysis and measurements for multiparameter radars. *J. Atmos. Oceanic Technol.*, **10**, 674–683.
- Hubbert, J., S. Ellis, M. Dixon, and G. Meymaris, 2010a: Modeling, error analysis and evaluation of dual polarization variables obtained from simultaneous horizontal and vertical polarization transmit radar. Part II: Experimental data. *J. Atmos. Oceanic Technol.*, **27**, 1599–1607.
- Hubbert, J. C., 2017: Differential reflectivity calibration and antenna temperature. *J. Atmos. Oceanic Technol.*, doi.org/10.1175/JTECH-D-16-0218.1.
- Hubbert, J. C., S. Ellis, M. Dixon, and G. Meymaris, 2010b: Modeling, error analysis and evaluation of dual polarization variables obtained from simultaneous horizontal and vertical polarization transmit radar. Part I: Modeling and antenna errors. *J. Atmos. Oceanic Technol.*, **27**, 1583–1598.
- Ice, R. L., A. K. Heck, J. G. Cunningham, and W. D. Zittel: 2014, Challenges of polarimetric weather radar calibration. *ERAD 2014*, Garmisch-Partenkirchen, Germany.
- Tapping, K.: 2001, Antenna calibration using the 10.7 cm solar flux. *Radar Polarimetry for geoscience applications*, P. Smith, ed., American Meteorological Society, [http://cdserver.ametsoc.org/cd/010430\\_1/RADCAL\\_Links\\_2\\_Presentations.html](http://cdserver.ametsoc.org/cd/010430_1/RADCAL_Links_2_Presentations.html).
- Wang, Y. and V. Chandrasekar, 2006: Polarization isolation requirements for linear dual-polarization weather radar in simultaneous transmission mode of operation. *IEEE Trans. Geosc. and Remote Sen.*, **44**, 2019–2028.

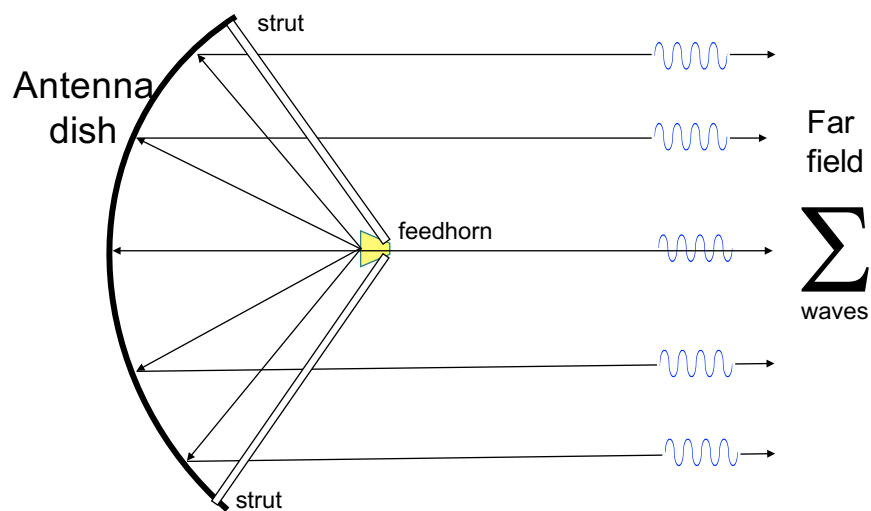


Figure 1: A sketch illustrating the combination of the electric field wave from the feed horn reflected by the dish. The far field is a combination of the waves. The nature of the resulting far field antenna pattern depends directly on the phase relationship of the waves.

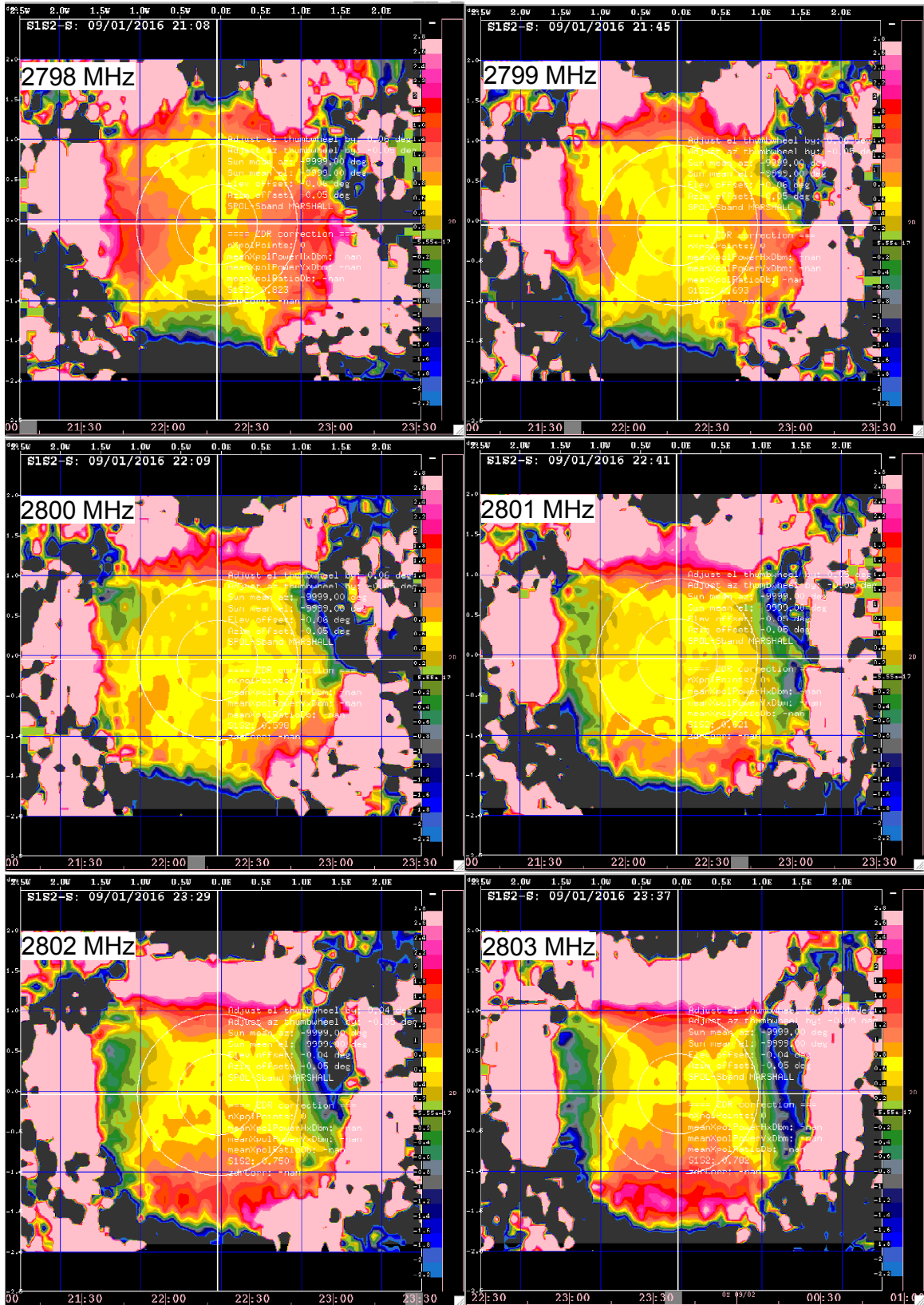


Figure 2: A series of  $S_1 S_2$  S-Pol antenna patterns from data gathered on 1 September 2016 at frequencies 2798 to 2803 MHz. The grid spacing is 0.1 deg. in both elevation (vertical axis) and azimuth (horizontal axis). The accompanying  $S_1 S_2$  averaged over a 1 deg. solid angle (the shown inner white circle) is given in Fig. 4.

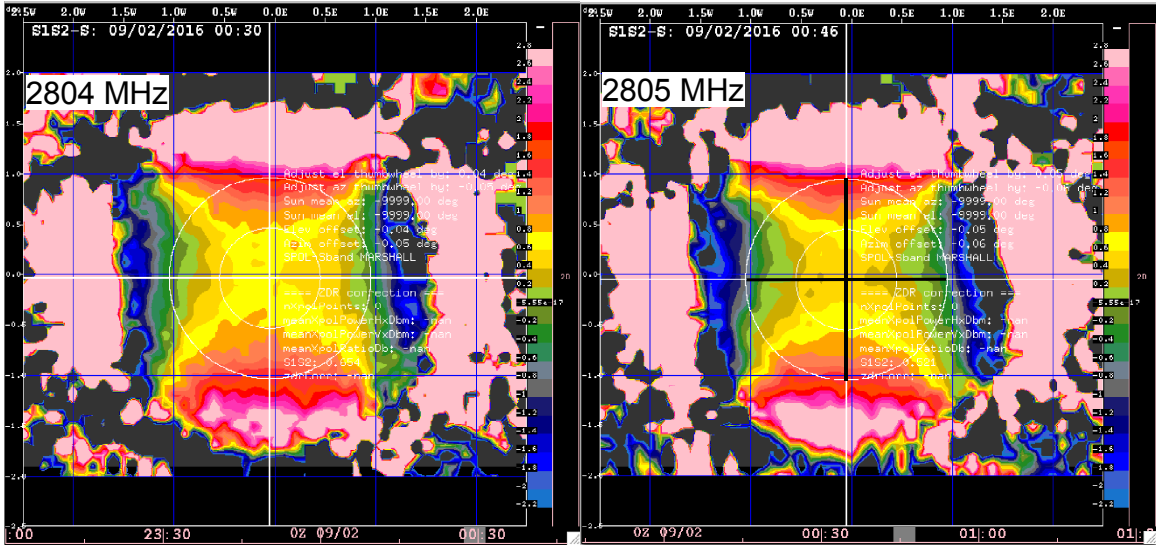


Figure 3: As in Fig. 2 for frequencies 2804 and 2805 MHz.

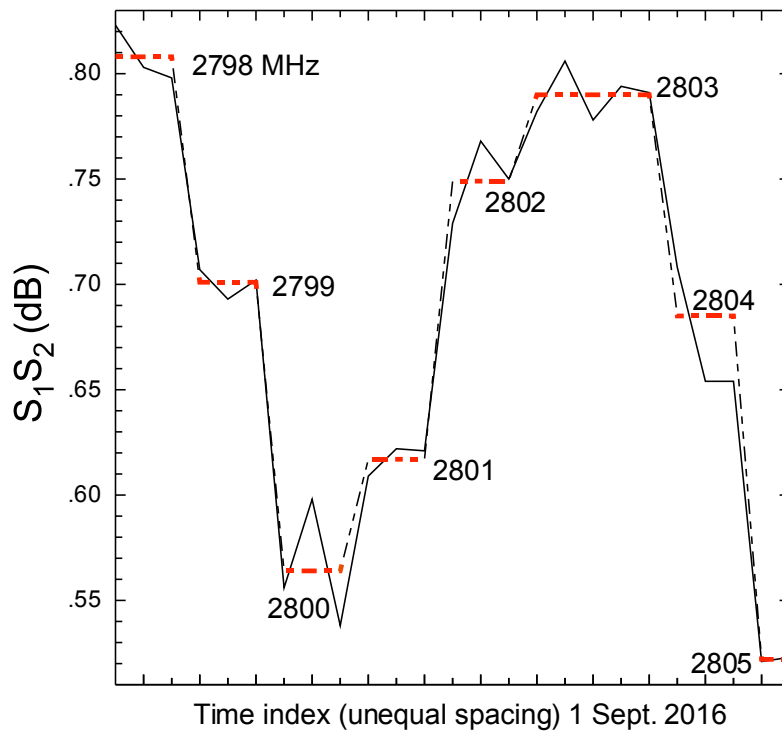


Figure 4:  $S_1 S_2$  versus frequency of operation for S-Pol. Data gathered on 1 September 2016 from 15:00 to 18:10 local time. The dashed red lines represent the average of  $S_1 S_2$  from the solar scans at each frequency. At least 3 solar scans were executed at each frequency except 2805MHz.



Figure 5: *S-pol antenna surface measurements .*

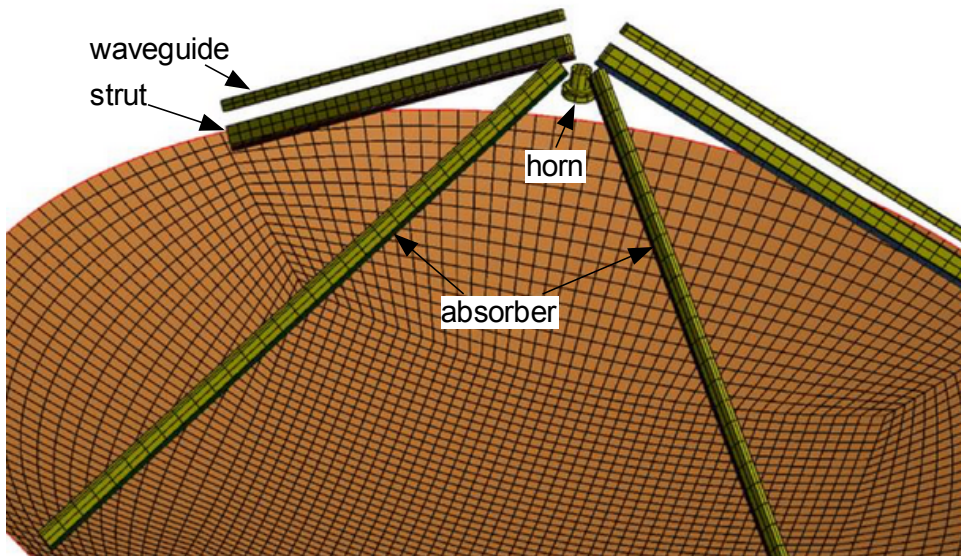


Figure 6: *S-pol antenna TICRA modeling topology.*

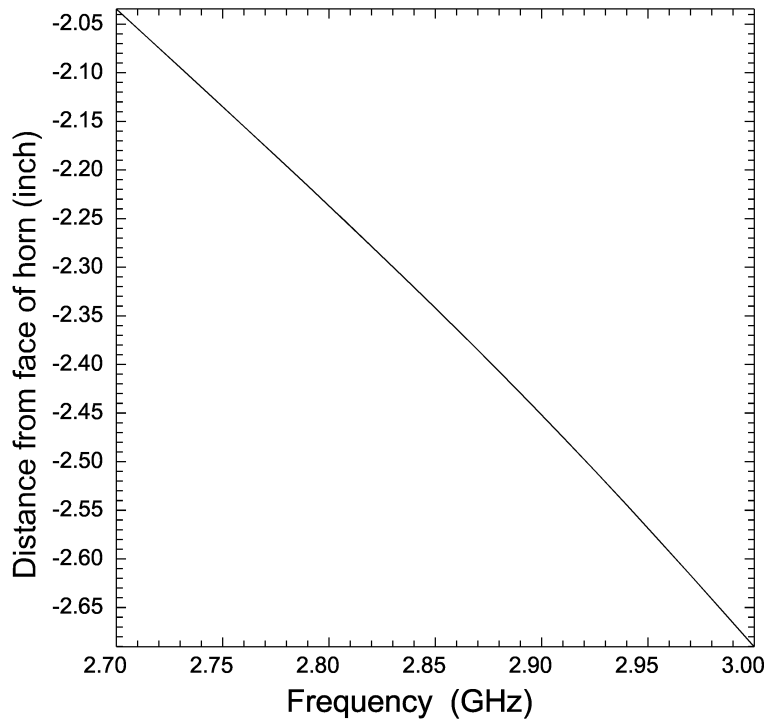


Figure 7: Phase center of S-Pol's feed horn as a function of frequency. S-Pol's typical operating frequency is 2809 MHz.

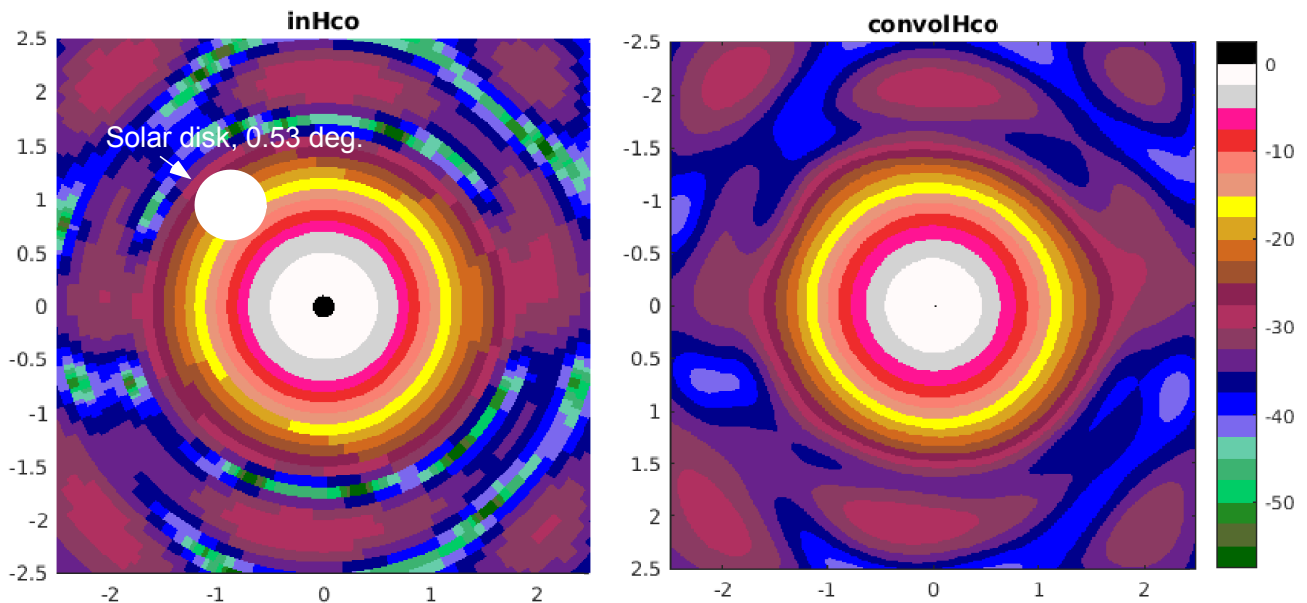


Figure 8: H-coplar modeled antenna pattern. The dB scale is normalized to the maximum power. Shown is a white disk ( $0.53^\circ$  diameter) that represents the sun. To accurately compare the TICRA modeled antenna patterns to the S-Pol experimental solar patterns, the modeled antenna pattern must be convolved with the solar disk. That is shown in the right panel.

**Feed=147.25in WP1200 convol ZDR bias Freq 2801-2806**

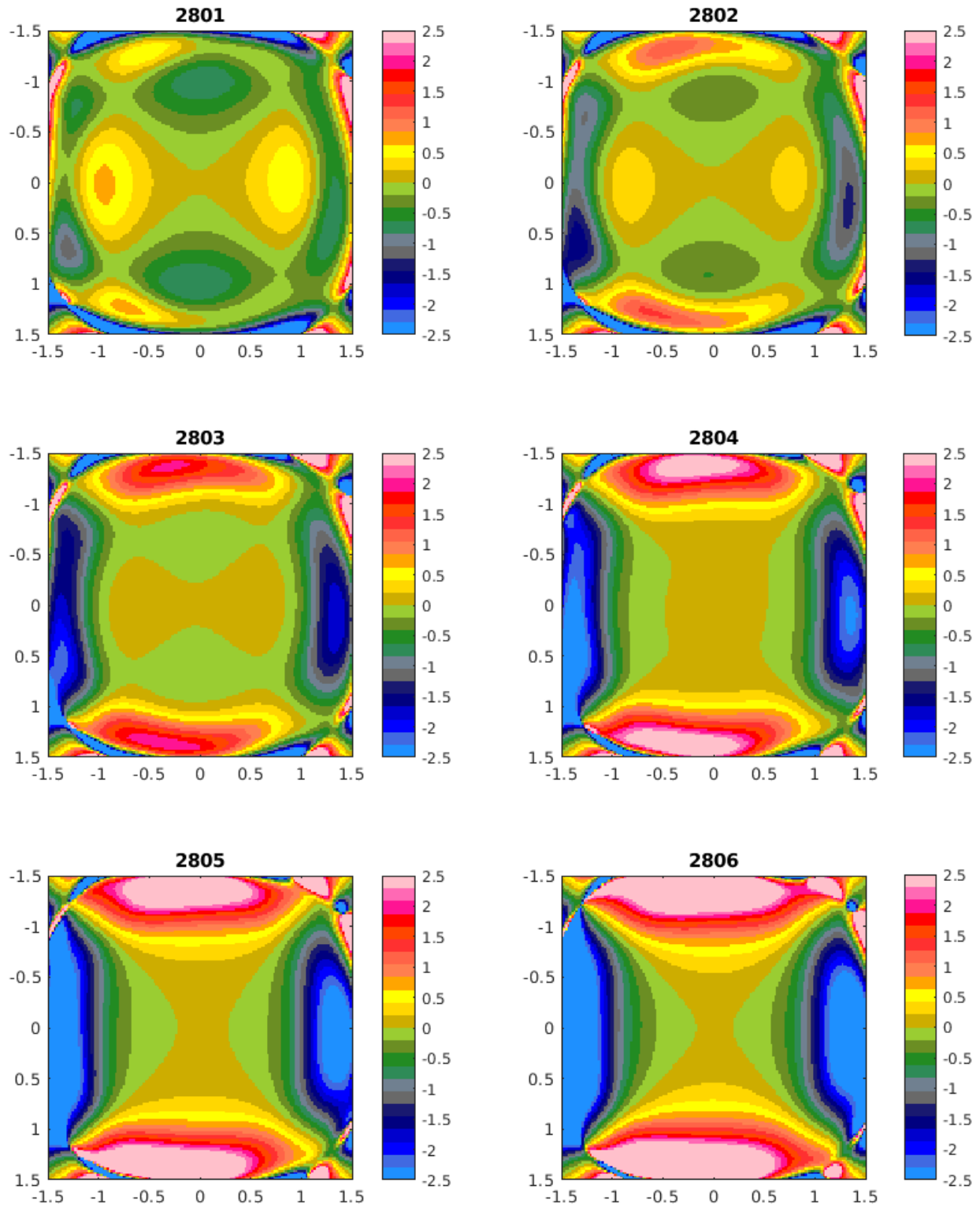


Figure 9:  $Z_{DR}^b$  antenna pattern convolved with the solar disk. Full model, i.e., with waveguide and strut absorber. Frequencies 2801 to 2806 MHz

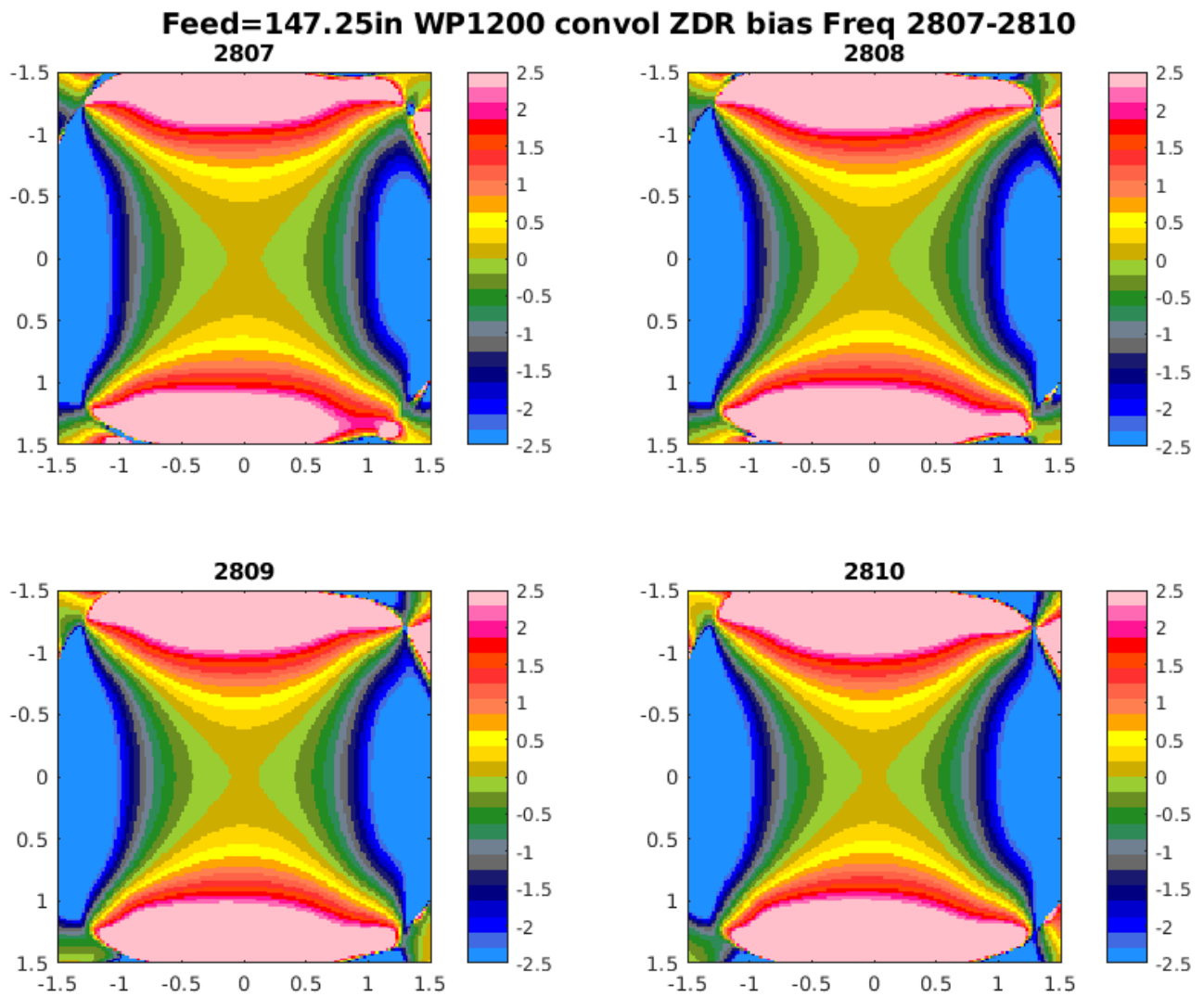


Figure 10: As in Fig. 9 for frequencies 2807 to 2810 MHz.

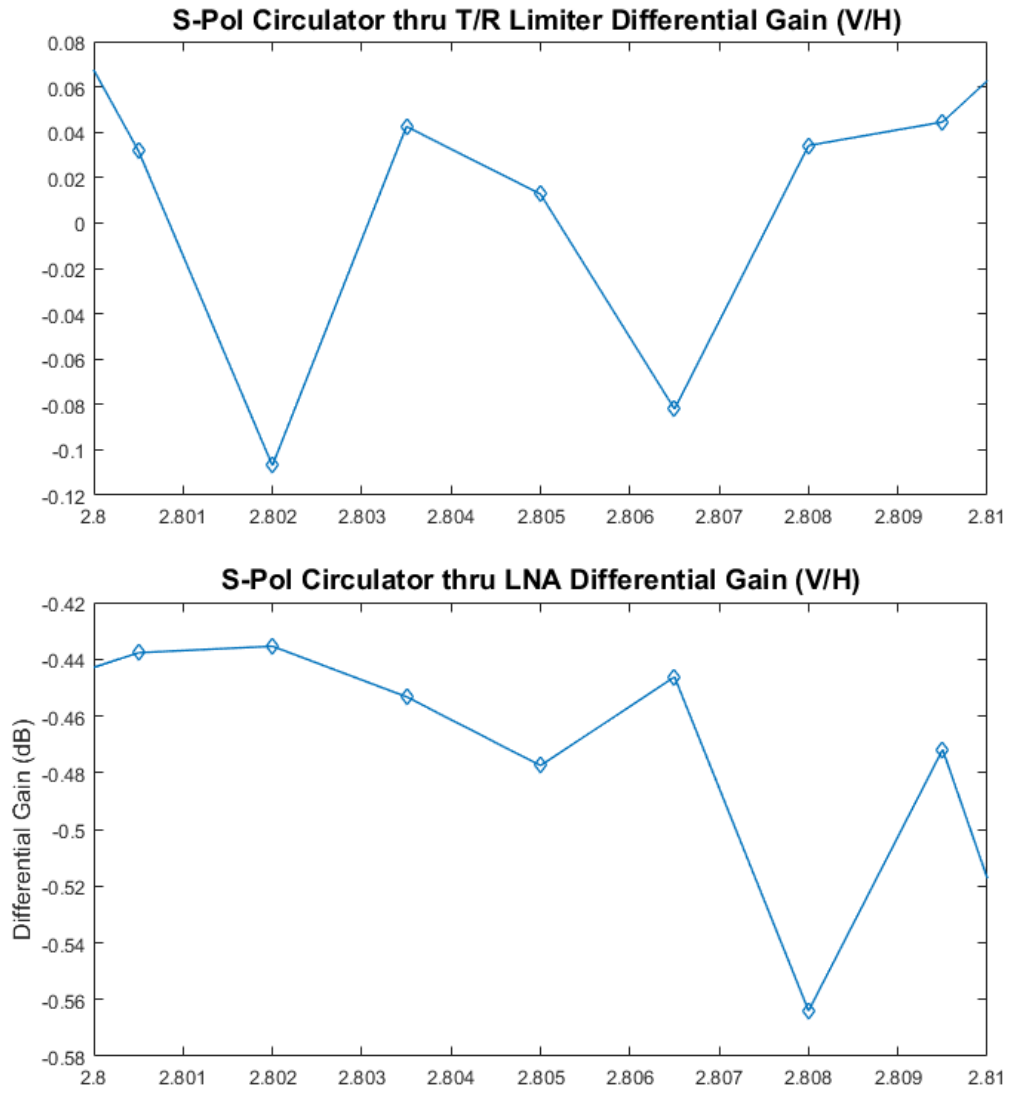


Figure 11: *V to H Differential gain of the H and V LNAs and circulators,  $C_{H,V}^R$ .*

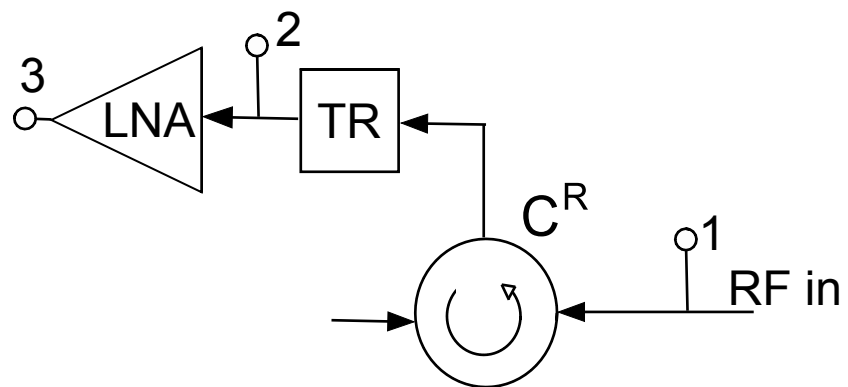


Figure 12: Block diagram of S-Pol's H or V RF receive path with TR (TR limiter). These components likely have a frequency dependent gain.

**Feed=147.25in WP1200 ticra ICPR num by fHH^2 Freq 2801-2806**

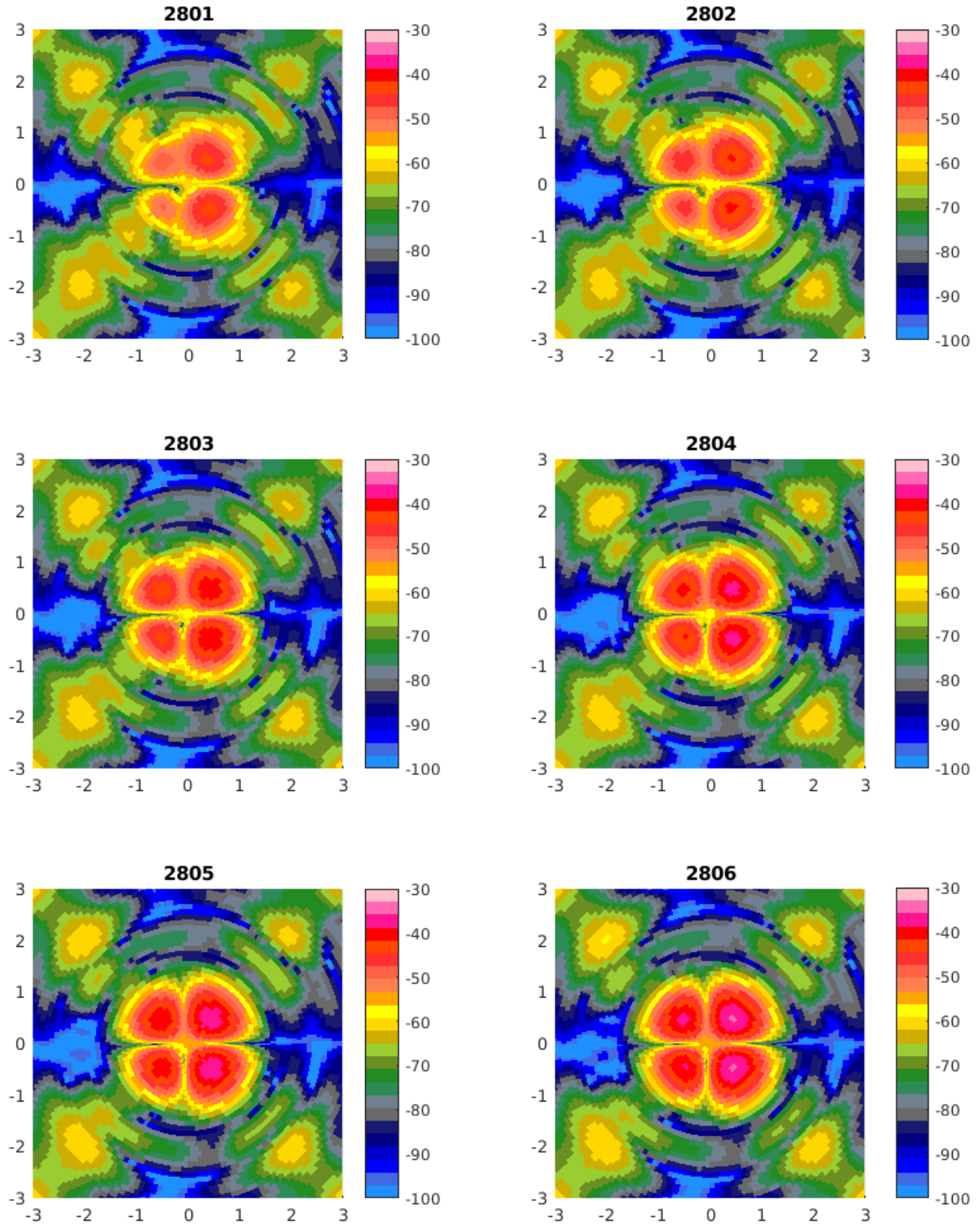


Figure 13: *ICPR* antenna patterns as calculated from the *TICRA* modeled antenna patterns (not convolved with solar disk) using Eq.(3), as a function of frequency from 2801 to 2806 MHz. Phase center of the feed horn is at 149.51 in from the dish. *H* and *V* axes are in degrees. The color scale is in dB.

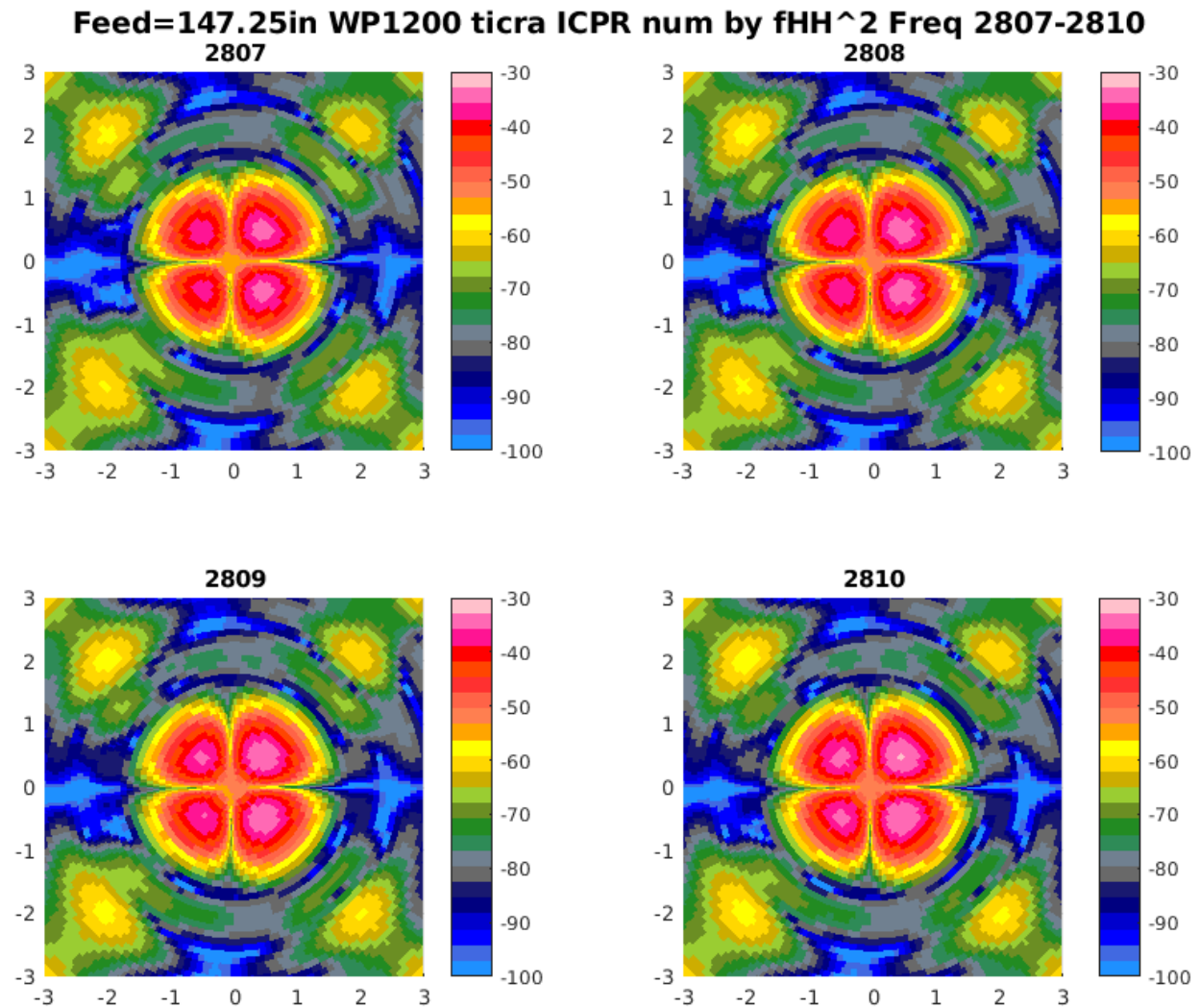


Figure 14: As in Fig. 13, ICPR antenna patterns as calculated from the TICRA modeled antenna patterns using Eq.(3), as a function of frequency from 2807 to 2810 MHz. Phase center of the feed horn is at 149.51 in. from the dish. H and V axes are in degrees. The color scale is in dB.

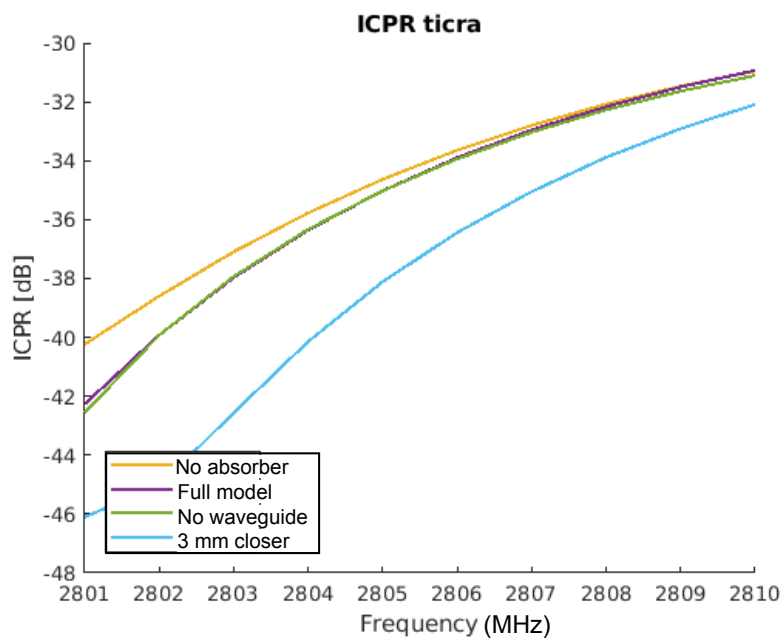


Figure 15: *ICPR* as calculated from the TICRA modeled antenna patterns (not convolved with solar disk) using Eq.(3) for the 4 cases as a function of frequency from 2801 to 2810 MHz. Phase center of the feed horn is at 149.51 in. from the dish.